Geochemistry Geophysics Geosystems G3
AN ELECTRONIC JOURNAL OF THE EARTH SCIENCES
Published by AGU and the Geochemical Society

Research Letter
Volume 5, Number 3
11 March 2004
Q03004, doi:10.1029/2003GC000520
ISSN: 1525-2027

Strong directivity of ocean-generated seismic noise

Vera Schulte-Pelkum
Cooperative Institute for Research in Environmental Sciences (CIRES), University of Colorado, Boulder, Colorado 80309, USA (vera_sp@cires.colorado.edu)

Paul S. Earle
U.S. Geological Survey, DFC, Box 25046, MS 966, Denver, Colorado 80225, USA

Frank L. Vernon
Institute for Geophysics and Planetary Physics, University of California, San Diego, A-0225, 9500 Gilman Drive, La Jolla, California 92093, USA

[1] We measure direction and amplitude of ocean-generated continuous seismic noise in the western United States. Slowness direction of the noise is determined using array beamforming, and particle motion direction from individual three-component stations. We find two surprising results. First, the noise is highly monodirectional at all sites, regardless of coastal distance. A single narrow generation area dominates for most of the time period, interrupted by a second well defined direction during ocean swell events. Second, we find that a storm off the Labrador coast with not unusual wave heights generates coherent noise across the entire continent. We show the causal relationship between swells arriving at different North American coastal areas and the triggered microseisms in time-lapse movies (Animations 1 and 2) of ocean swells and concurrent microseisms. Our results have a number of implications for different fields of research. A useful by-product of our finding that microseisms are a strongly directional noise source is the possibility of using automated processing of the continuous noise as a near real-time check on station polarity and calibration problems, which would be a simply implemented indicator for the state of health of a seismic network. Consistent monodirectional noise may have an influence on seismic azimuthal measurements such as shear wave splitting. Most importantly, our findings should be taken into account in proposed studies which will use seismic noise as a proxy for ocean wave height in investigations of interdecadal climate change.

Components: 4122 words, 8 figures, 2 movies.

Keywords: Ocean microseisms; climate change; seismic networks.

Index Terms: 1635 Global Change: Oceans (4203); 4215 Oceanography: General: Climate and interannual variability (3309); 7255 Seismology: Surface waves and free oscillations.

Received 7 February 2003; **Revised** 6 November 2003; **Accepted** 15 December 2003; **Published** 11 March 2004.

Schulte-Pelkum, V., P. S. Earle, and F. L. Vernon (2004), Strong directivity of ocean-generated seismic noise, *Geochem. Geophys. Geosyst.*, *5*, Q03004, doi:10.1029/2003GC000520.

1. Introduction

[2] Ocean swells generate a continuous seismic signal on land, referred to as microseisms. Microseisms are found in two distinct frequency bands. Single frequency microseisms occur at the predominant swell frequency (typically 0.07–0.1 Hz, corresponding period 10–14 s) and double fre-

quency microseisms are seen at twice the swell frequency (typically 0.14–0.2 Hz, corresponding period 5–7 s). The generation mechanism of the single frequency microseisms is not well understood, but likely involves direct interaction of the swell with a shallow seafloor or the shore [*Hasselmann*, 1963]. The higher-energy double frequency signal is generated by nonlinear interaction between two opposing wave fields [*Longuet-Higgins*, 1950], predominantly set up by reflection off a coastline [*Haubrich and McCamy*, 1969].

[3] Recent studies have investigated the possibility of using the amplitude of microseisms as a proxy for ocean wave height [*Bromirski et al.*, 1999; *Grevemeyer et al.*, 2000]. The motivation behind these studies is that seismic records predate buoy measurements by decades, so that seismic estimates of ocean wave height would provide a much longer time series for an investigation of ocean climate change. The inherent assumption is that microseism amplitudes at a land station reflect the ocean wave height averaged over a regional source area. Here, we investigate the validity of this assumption by studying directional data. A thorough historical study would require a major effort including digitization of paper records and has to date not yet been conducted. Preliminary investigations such as we present here will aid in the planning of such a project.

2. Seismic Data and Methods

[4] We analyzed continuous noise recorded at land stations in the microseism band in the western United States for a randomly selected three-week time period (12–31 January 1998). Continuous noise records were taken from the Terrascope broadband seismic network [*Mori et al.*, 1998], six broadband stations from other networks, and from the Anza broadband array (http://eqinfo.ucsd.edu/deployments/anza.html), all archived at the IRIS Data Management Center. We used the archived continuous LH (1 Hz) channels at all stations. Station locations are shown in Figure 1.

[5] Microseisms are thought to propagate predominantly as Rayleigh waves (surface waves with retrograde elliptical motion in the vertical plane) in the Earth's crust [*Haubrich and McCamy*, 1969]. We measure the direction of approach of microseisms in the single and double frequency band. At each of the network stations, we determine the amplitude and direction of approach of the continuous noise by polarization analysis of the continuous three-component record, using a time domain covariance method [*Jurkevics*, 1988; *Earle*, 1999]. We filter the continuous noise records with a bandpass bracketing the double frequency peak (0.1–0.5 Hz). The particle motion is estimated in 15 minute windows. We limit the network station analysis to the double frequency microseism band, since the particle motion of the lower amplitude single frequency microseisms is less well determined. There are some data gaps, particularly on 20 January for which day Terrascope network data are missing in the archive.

[6] At the array, we measure the azimuth and slowness of the microseisms by finding the peak power in slowness space in linear time domain slant-stacks of the continuous vertical seismograms [*McNamara and Owens*, 1993]. The beamforming is applied after filtering the data to the microseism band (0.1–0.5 Hz for double frequency, 0.05–0.1 Hz for single frequency microseisms). Beam estimates are formed for 15-minute time windows. The signal in both bands is highly coherent across the array and typically shows a single well-defined peak in each band, at slownesses corresponding to that of crustal Rayleigh waves (~0.3 s/km). During brief time intervals, two slowness peaks are visible. We track the highest power peak and thus pick out the generation area for the strongest microseisms. In contrast, the single station polarization analysis averages over source azimuths when more than one source exists.

3. Seismic Results

[7] Figure 2 shows the continuous noise amplitude at the network stations and the peak noise power at the Anza array in the double frequency microseism band. The correlation between station particle motion amplitude and array peak power is extremely high. High amplitudes occur around 14, 21, 23, 31 January. A sharp amplitude peak late on January

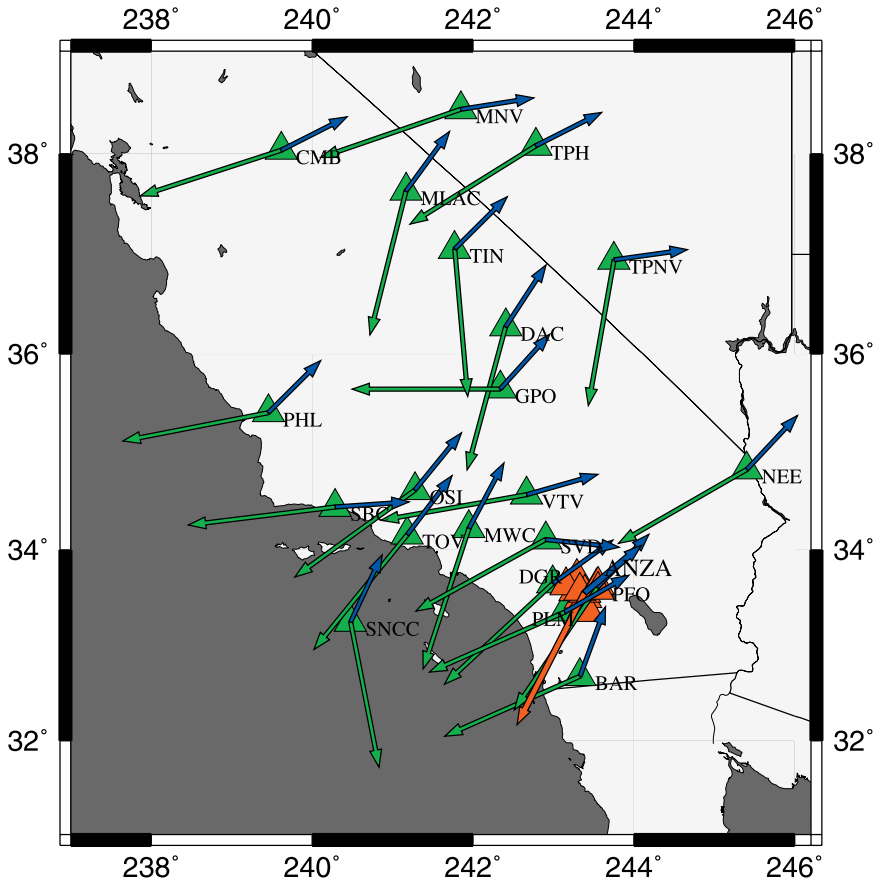

Figure 1. Locations of network stations (green) and Anza array (red). Base noise azimuths in the double frequency microseism band are shown as a red arrow at Anza and as green arrows at the stations. Blue arrows show the direction during the azimuth flip on January 23–24. Polarity errors at BAR and OSI have been corrected. Station SVD may have an orientation problem.

12 is a m_b 6.4 Chilean earthquake. One noise peak (around the 23rd) occurs simultaneously at all locations, while the peaks around the 14th, 21st, and 31st arrive later in that south than in the north. We explain this behavior through correlation with ocean swell events in a later section.

[8] The direction of the continuous noise measured using array slowness (Figure 3, top) shows a surprising modal behavior. The noise azimuth locks onto fixed directions for days at a time. There is a predominant base azimuth of SSW, interrupted by shorter periods of a W azimuth and one of a NE azimuth. During times of locked noise azimuth (e.g., day 14–15 and 21–22), the standard deviation is less than 10°. Similar modal noise backazimuth behavior has been observed at the Gräfenberg array in Germany [*Friedrich et al.*, 1998].

[9] Station particle motion azimuths (Figure 3) show more scatter, but the azimuth switches are also visible. The amount of azimuth scatter varies strongly from station to station. Stations BAR and OSI show large azimuth discrepancies relative to all other stations. Subsequent analysis of large teleseismic events from the study period confirmed polarity errors during our study period in the north component at BAR and in the east component at

Figure 2. Array peak power (red, top) and normalized station noise amplitudes (blue) in the double frequency microseism band. Stations are sorted in order of increasing latitude, from south to north. The array isolates the highest amplitude noise source, while the stations average over all active sources. Owing to higher scatter in the station azimuth estimates, we applied a 5-point median filter (not used for the array).

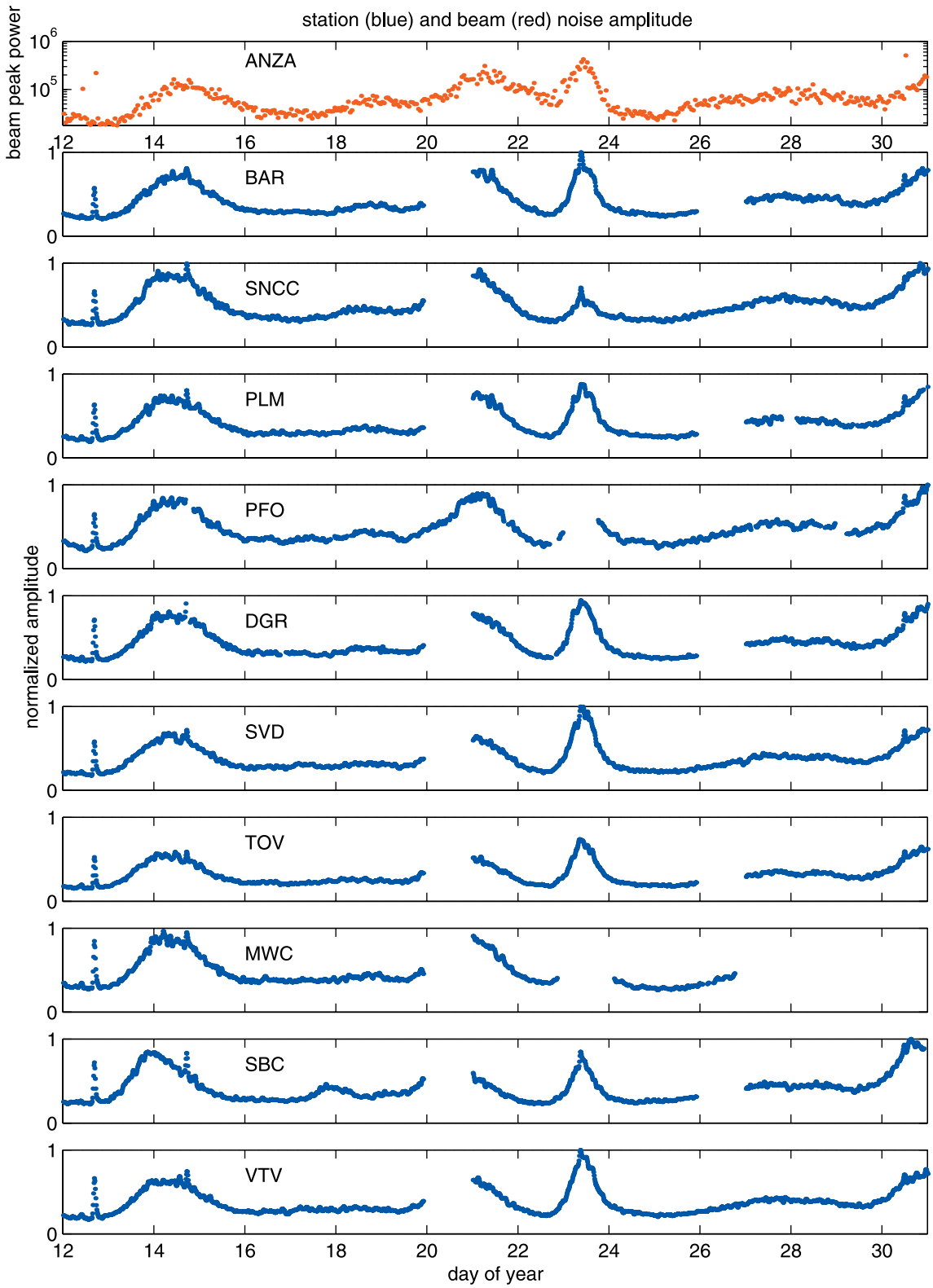
station (blue) and beam (red) noise amplitude
beam peak power
10^6
10^5
ANZA
12
14
16
18
20
22
24
26
28
30
normalized amplitude
1
0
BAR
SNCC
PLM
PFO
DGR
SVD
TOV
MWC
SBC
VTV
day of year

Figure 2.

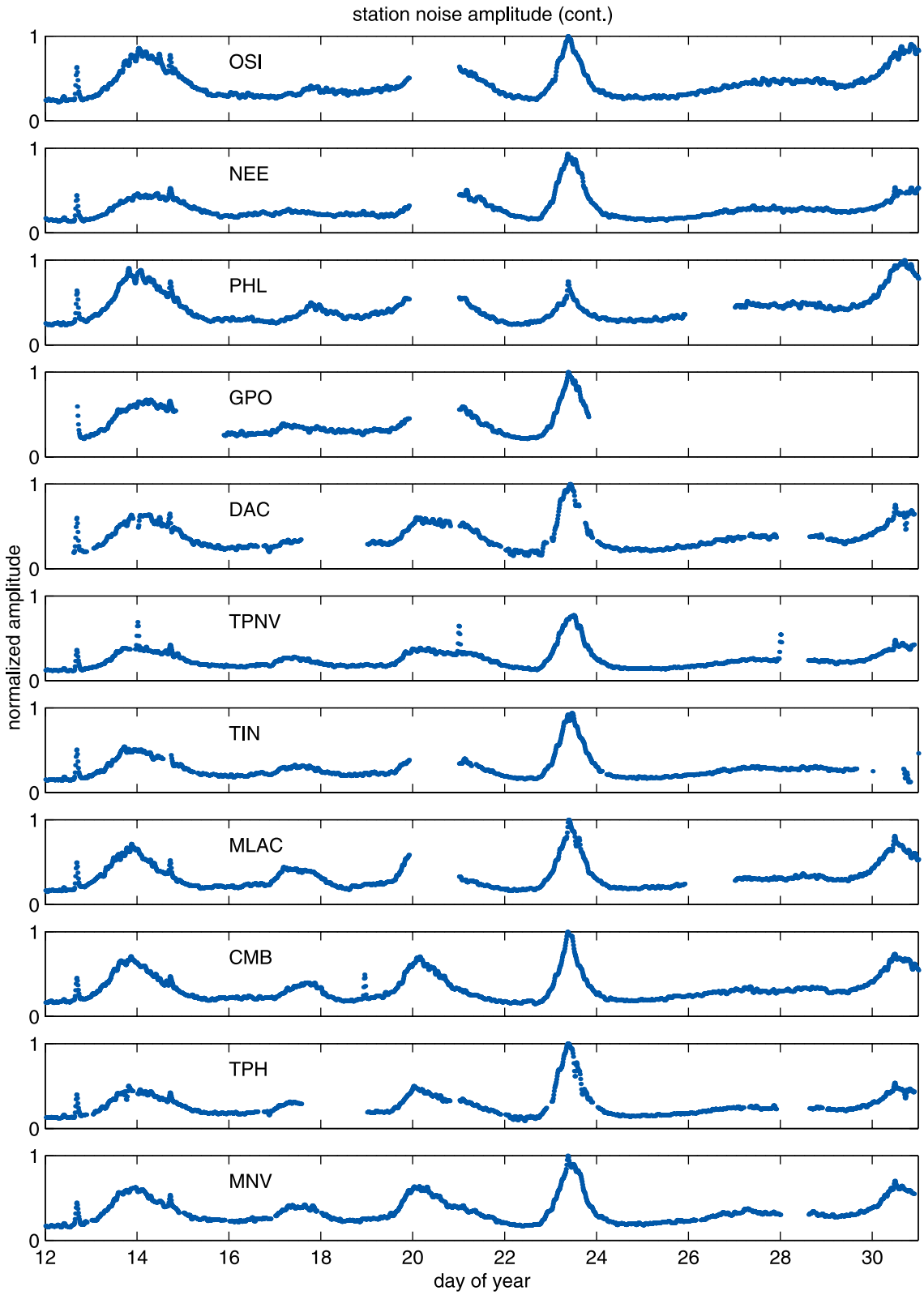

Figure 2. (continued)

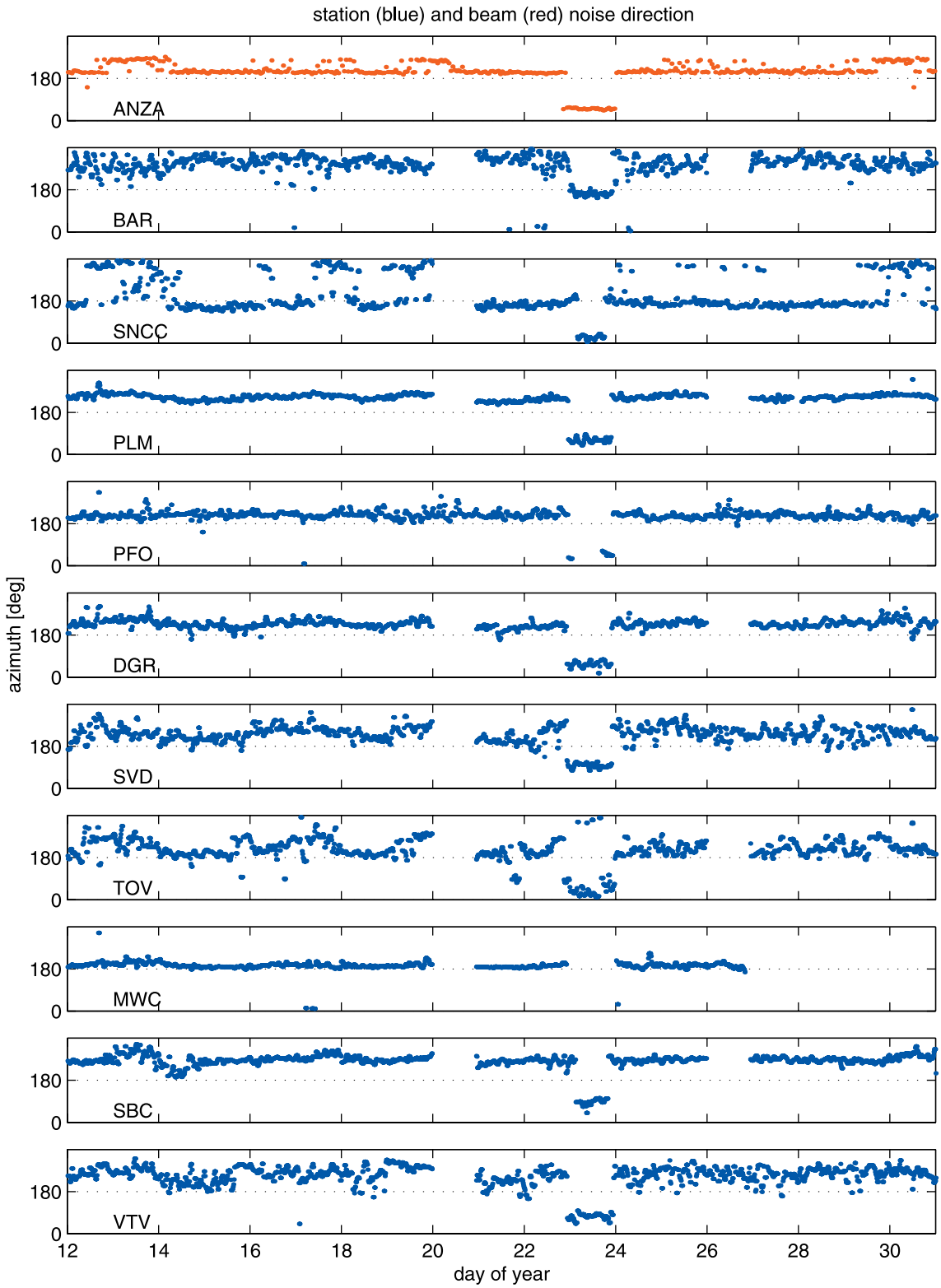

Figure 3. Array peak power azimuth (red, top) and stations particle motion azimuths (blue) in the double frequency microseism band. Stations are sorted in order of increasing latitude, from south to north. The array locates the highest amplitude noise source, while the stations average over all active sources. Stations BAR and OSI have obvious polarity problems.

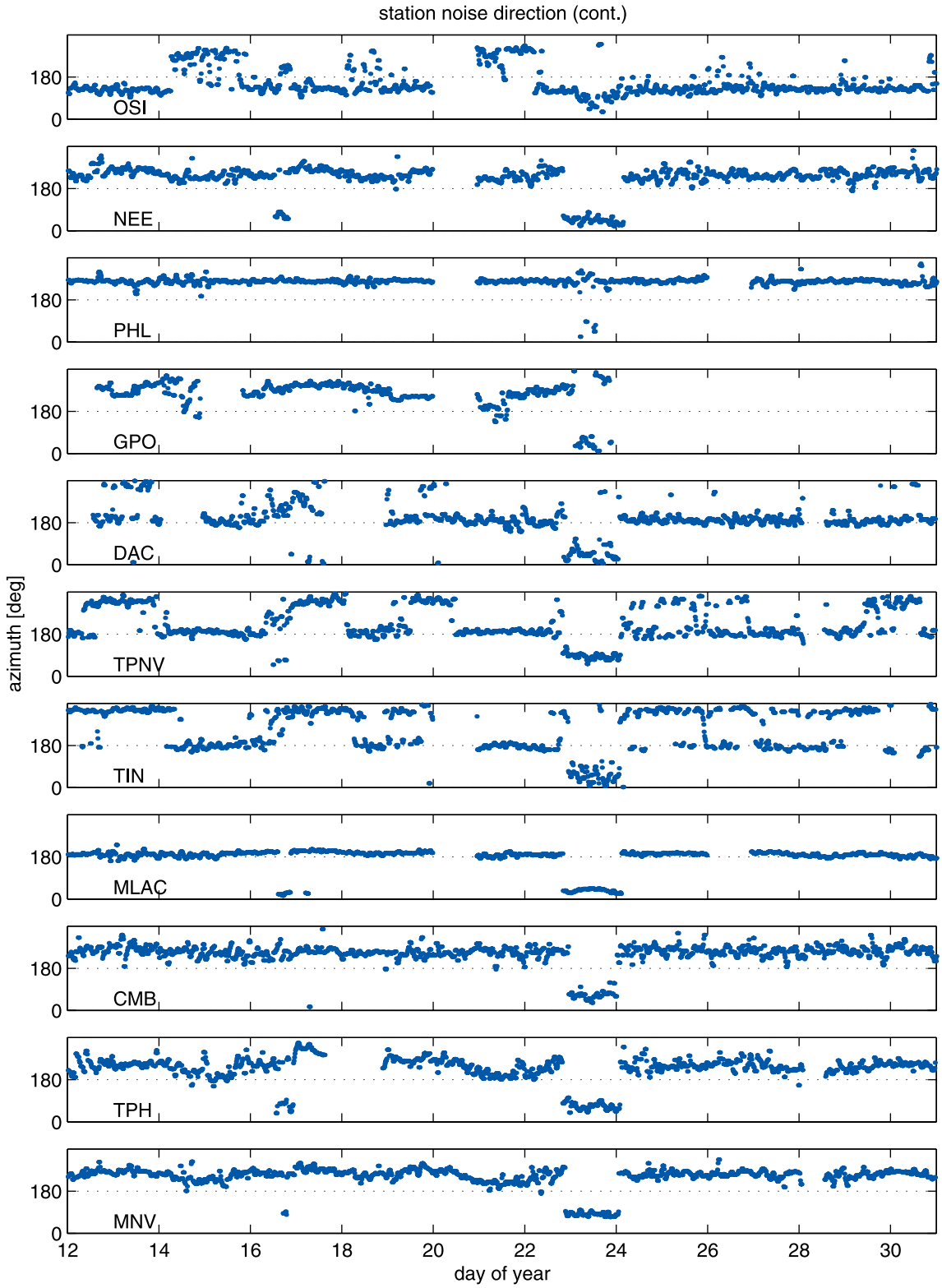

Figure 3. (continued)

OSI. All stations show northeast azimuths on 23 January. Comparing Figures 2 and 3, azimuth switches appear to coincide with or slightly precede amplitude peaks.

[10] Measured noise azimuths in the double frequency microseism band are also plotted in Figure 1 (with corrections for polarity errors). We show the base azimuth as well as the azimuth during 23–24 January. The base azimuth at most southern stations points to offshore of the southern California bight. Surprisingly, a group of northern stations (MLAC, TIN, TPNV, DAC) have southerly base azimuths which also point to this area. This may be due to seismic propagation effects [*Harben and Hjortenberg*, 1993]. All other northern stations have base azimuths pointing west toward offshore central California. The NE azimuth at the Anza array lies on the great circle path to the Labrador coast. Note the good agreement between Anza slowness and the colocated PFO particle motion directions for both base and NE azimuth.

4. Comparison With Ocean Data and Discussion

[11] To determine the source of the continuous noise, we compare ocean wave height data to our seismic results. We use three types of wave height data: recordings from California coastal buoys, a regional model seeded from recordings from a deep water buoy, and wind-based regional and global wave models.

[12] The buoys log wave height, predominant period and direction at half-hourly intervals and provide spot measurements of the swell field. Since most buoys are relatively close to shore and the shallow water depth modifies the swell, we also use an hourly southern California bight swell hindcast seeded from the deeper water (204 m) Harvest Platform directional buoy that includes refraction and diffraction effects due to coastal shape and islands (CDIP regional swell model, *O'Reilly and Guza* [1993]), and three-hourly global and regional swell hindcasts based on forcing by NCEP/NCAR reanalysis winds (NCEP WAVEWATCH III model, *Tolman* [1999]).

[13] We first relate the noise amplitude peaks and azimuth switches to swell events. By theory, land noise amplitude should be proportional to the swell energy [*Kibblewhite and Ewans*, 1985]. Figure 4 shows array beam peak noise amplitude and azimuth in the double frequency microseism band and wave energy at 33° N/240° E from a regional hindcast based on NCEP/NCAR reanalysis winds in a range of periods. Red arrows indicate the timing of noise peaks, blue arrows the timing of noise azimuth switches from SSW to W. We have omitted the noise peak and azimuth switch on day 23, as we will show later that it is not related to wave activity in the Pacific. The noise peaks show good correspondence with peaks in wave energy at 15 s (equivalent period for double frequency microseisms 7.5 s), while the azimuth switches coincide with the arrival of 22 s wave energy (corresponding double frequency microseism period 11 s). The band filter applied to the seismic data with corner periods of 2 and 10 s contains the corresponding wave periods. Owing to the dispersion of water waves, longer period wave energy precedes shorter period wave energy, which is visible in the middle frame in Figure 4. The amount of dispersion depends on the distance traveled by the swell. Noise azimuth switches (blue arrows) similarly precede noise maxima (red arrows). The three highest noise maxima are preceded by the three most consistent azimuth switches (first, third, and fifth arrow each from the left).

[14] While a quantitative correlation between noise and wave energy would be desirable, we lack the wave data to do so. The wave heights used in Figure 4 are calculated from wind-forcing for a point in the open ocean. Refraction and shadowing effects due to the coast and islands are not included in the model. Direct buoy measurements are from shallow water, which strongly modifies the waves at the periods considered here. The regional model published by CDIP includes refraction and shadowing effects, and is seeded from deep water data from the Harvest Platform. However, these regional models show an instantaneous response of the wave field in the bight to conditions at Harvest Platform and do not account for finite travel times

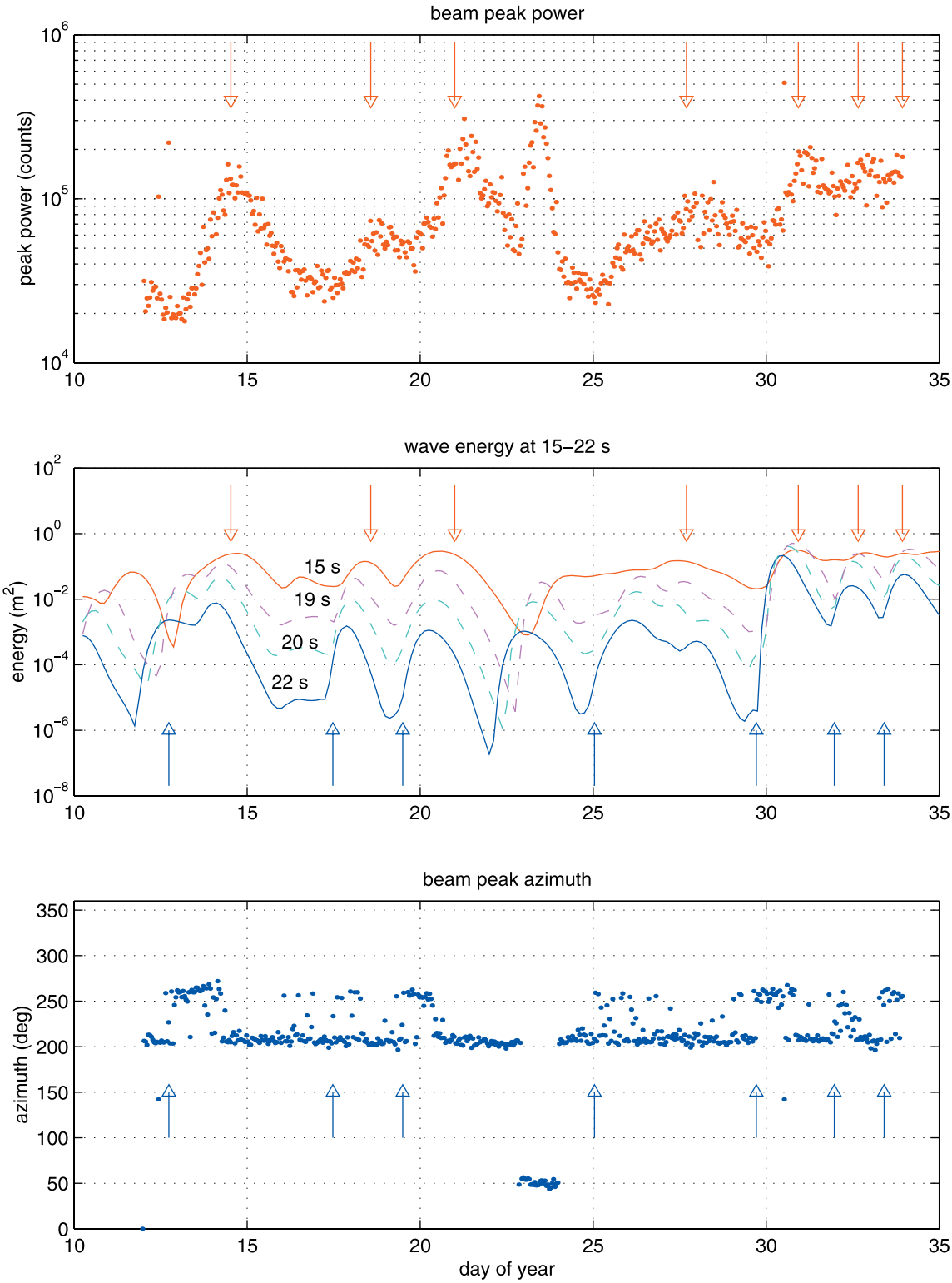

Figure 4. Correspondence between double frequency microseism amplitude given by Anza beam peak power (top), wave energy for deep water at 33° N/240° E in a range of periods (middle), and Anza beam peak azimuth (bottom). Red arrows indicate timing of noise maxima, blue arrows timing of azimuth switches.

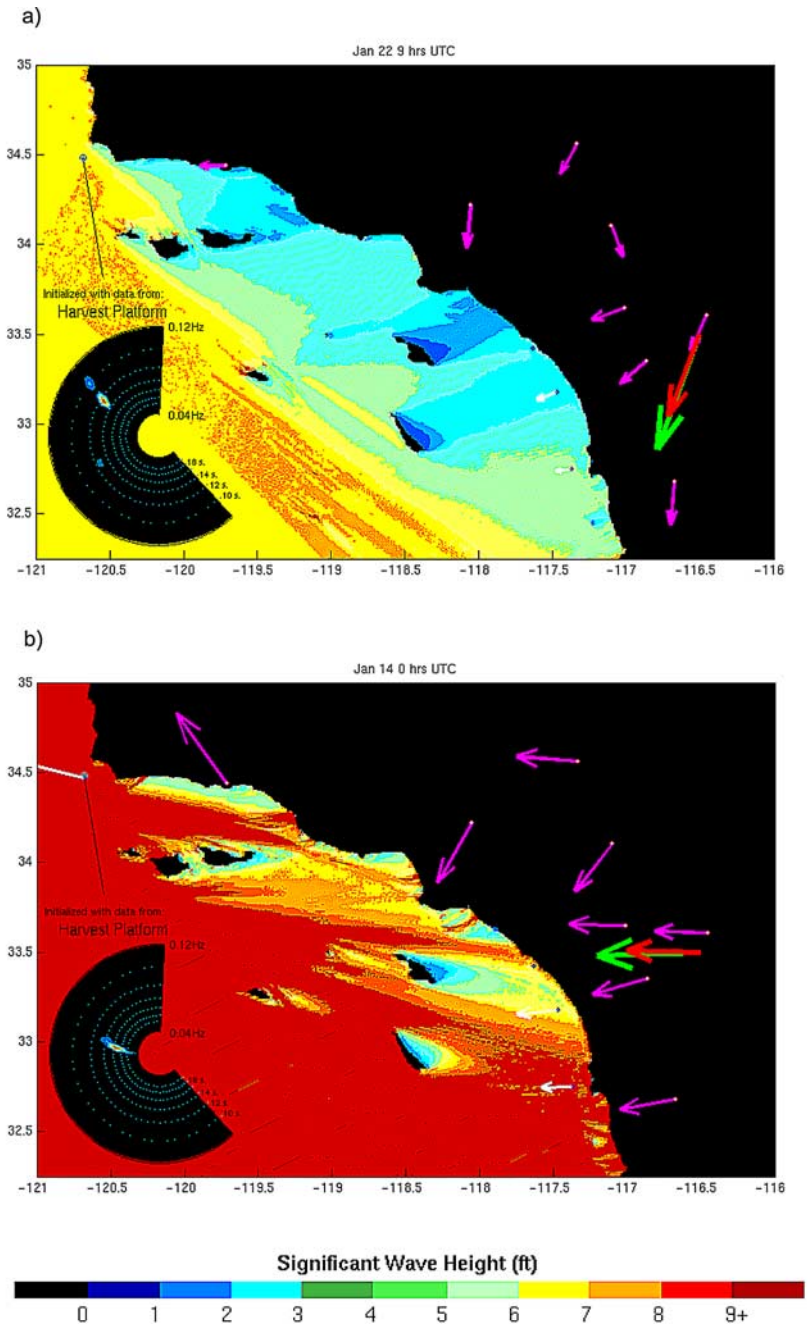

Figure 5. Array beam azimuths (red arrow-single frequency, green arrow-double frequency microseisms), station polarization and amplitude of double frequency microseisms (magenta arrows), buoy swell directions and energy (grey arrows; swell energy scales with double frequency microseism amplitude by theory), and CDIP model wave heights. The wave heights are calculated from buoy data at the Harvest Platform using refraction and diffraction modeling [*O'Reilly and Guza*, 1993]. The directional wave spectrum at the Harvest buoy is shown in the inset. See Animation 1 for all frames (See the HTML version of the article available at http://www.g-cubed.org). (top) Frame during the base SSW microseism state, (bottom) frame during a W microseism azimuth state triggered by a western swell.

of waves from the buoy location to points on the coast, which leads to an error in timing on the order of half a day for swell propagation through our study area.

[15] Figure 5 shows two frames from a movie generated by combining hourly regional wave maps seeded from Harvest buoy data, the directional wave spectrum at the Harvest Platform, microseism direc-

tions and amplitudes at the seismic stations, and coastal buoy wave heights. The top frame (day 22) is representative for the base SSW noise azimuth state, the bottom (day 14) for the W azimuth high noise state. The entire movie can be viewed in Animation 1 (regional movie). The Harvest Platform directional wave spectrum (insert in Figure 5 and in Animation 1) shows that the predominant wave direction during quiet periods is from the NW. Shadowing in the southern California bight is clearly apparent, and noise azimuths from southern California stations point toward a source area offshore Baja California and outside the bight's wave shadow. During swell events, the noise azimuths are sensitive to the arrival of long-period wave energy and switch from SSW to W, accompanied by a shift to low frequency waves from the W visible in the directional wave buoy spectrum. Swells from the west lead to higher amplitudes in the bight due to the lack of a wave shadow. The highest noise amplitudes are recorded after a delay once the higher energy, shorter period ocean waves arrive.

[16] The consistent NE noise azimuths around day 23, which are concurrent with the highest noise amplitudes, suggest that microseisms during that time period may be triggered by Atlantic rather than Pacific waves. We use global NCEP wave model data to verify this hypothesis. Figure 6 shows two frames from the resulting movie. The entire movie with the global wave model and array beam can be viewed in Animation 2. Our suspicion of an Atlantic wave event is confirmed by the observation of a swell arriving at the Labrador coast simultaneous to the noise azimuth flip to NE (Figure 6, bottom frame). A second interesting event is the triggering of noise in the single frequency microseism band initially in British Columbia, then migrating southwards along the coast, around day 17 (Figure 6, top frame). While the Labrador Coast swell event resulted in the highest noise amplitudes during our study period, its wave heights were not unusual. The maximum significant wave height during the peak in microseism amplitudes (23 January, 9 hrs UTC) is 10.7 m, a value that is frequently exceeded at other times during our study period (see Animation 2). As an additional comparison, the north Atlantic 29 October–2 November 1991 "perfect storm" of book and movie fame [*Junger*, 1999] had a maximum significant wave height of 12.0 m recorded at the Georges Bank buoy (buoy 44011, http://www.ndbc.noaa.gov/station_history.phtml?station=44011), yet did not generate microseism levels comparable to the Labrador event (Peter Bromirski, personal communication, 2000). Although the 1991 storm caused higher waves, its track was farther south [*Bromirski*, 2001], and resulting swells should have hit the North American coast in a different location and with presumably a different angle than the Labrador swell we observed. Therefore a direct correspondence between wave heights and microseism amplitudes may not always hold, and coupling from wave to seismic energy may depend on additional factors such as the location and angle of the waves relative to the coastline. A dependence of seismic noise levels on ocean wave direction has been observed in northern and central Europe by *Essen et al.* [2003]. They conclude that increasing seismic noise levels may not necessarily reflect higher waves, but may also be due to a change in storm tracks resulting in increased coupling of wave to seismic energy. A similar situation would hold for our study area. *Graham and Diaz* [2001] suggest that cyclones in the northeast Pacific may have shifted from northwesterly to more westerly tracks in the last half century. Such a shift in direction would affect the coupling into seismic noise due to the influence of the wave shadow of the southern California bight. In general, the effect of directional changes may pose a problem in ocean climate hindcast studies that attempt to use seismic noise amplitudes as a proxy for direct ocean measurements for the first half of the 20th century, for which buoy records are not available. Pilot studies for this kind of climate investigation have been published [*Bromirski et al.*, 1999; *Grevemeyer et al.*, 2000], but a full historical analysis has to date not been performed. Triggering of microseisms at continental distances such as we observed may also be a source of bias in climate change studies, since it violates the assumption that microseism amplitudes are representative of regional ocean wave heights. We found one such event by chance during a randomly

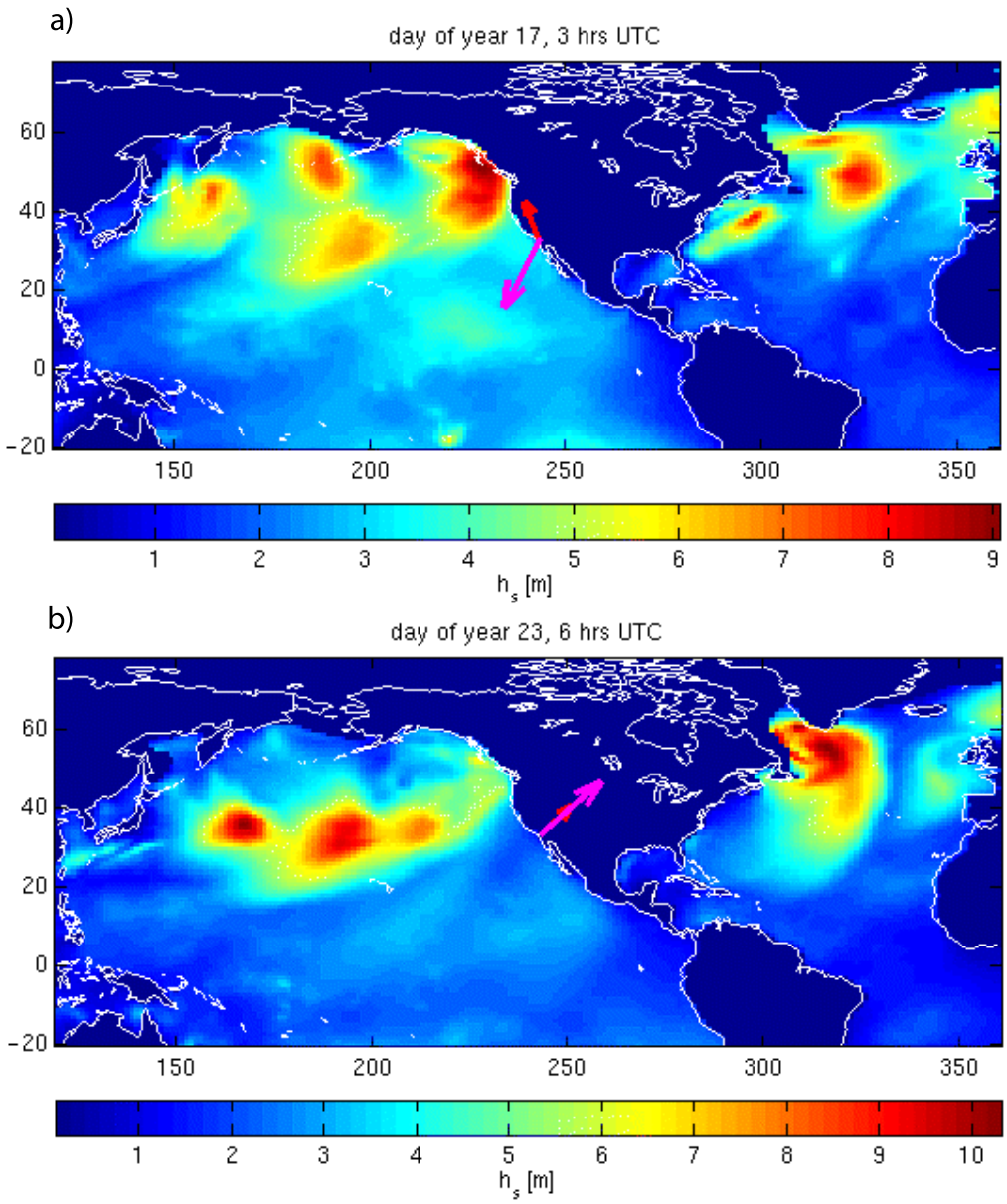

Figure 6. Wavewatch-III [*Tolman*, 1999] swell field and microseism beams. See Animation 2 for all frames. (top) As a large long-period swell hits the Canadian coast, the lower attenuation single frequency microseism beam (red arrow) switches to that azimuth (the beam great circle path intersects the BC coast) and tracks the swell along the coast to the south, while the double frequency microseisms (magenta arrow) stay on the local base SSW azimuth. (bottom) North Atlantic swell triggers transcontinental microseisms in both bands. The beam great circle path intersects the Labrador coast. See Animation 2 for all frames (See the HTML version of the article available at http://www.g-cubed.org).

selected three weeks; an investigation of how frequently transcontinental triggering occurs lies outside of the scope of this paper and would be an interesting exercise to perform elsewhere. However, if the assumption is that ocean storm behaviour may have undergone changes in the past century, then an absence of transcontinental triggering in the past can not be deduced even if it proves to be a rare event in the present. On the basis of our obserations, we conclude that directional analysis warrants further investigation in the context of ocean climate change studies.

[17] On a side note, the observation that seismic noise in the microseism band is highly directional opens up the possibility to use continuous noise as

a directional signal. We identified polarity errors at network stations in this study by comparing noise azimuths at adjacent stations. The same noise polarization analysis we used here could easily be applied automatically to network data on a continuous, near-real-time basis. Hourly averages of continuous noise azimuth and amplitude would provide an easily sifted indicator of the state of health of a seismic network. The implementation of such a process would be especially useful for cases where large amounts of seismic data are collected and archived on a regional basis, for instance in the case of the future USArray. On a second side note, the strong directionality of microseismic noise should also be addressed as a source of potential bias in directional seismic measurements. As an example, splitting (birefringence) of shear waves is commonly used to investigate anisotropy in the earth. Splitting analysis of the most commonly used phase, the core phase SKS, is usually conducted at frequencies that coincide with the high-amplitude noise double frequency microseism band, and an investigation on the effect of superposition of the split shear wave with consistently polarized noise on splitting measurements is desirable.

Acknowledgments

[18] We thank Nick Graham, William O'Reilly, Julie Thomas, and Hendrik Tolman for assistance with obtaining and interpreting wave data.

References

Bromirski, P. D. (2001), Vibrations from the ''Perfect Storm,'' *Geochem. Geophys. Geosyst.*, *2*, Paper number 2000GC000119.

Bromirski, P. D., R. E. Flick, and N. Graham (1999), Ocean wave height determined from inland seismometer data: Implications for investigating wave climate changes in the NE Pacific, *J. Geophys. Res.*, *104*, 20,753–20,766.

Earle, P. S. (1999), Polarization of the Earth's teleseismic wavefield, *Geophys. J. Int.*, *139*, 1–8.

Essen, H., F. Krüger, T. Dahm, and I. Grevemeyer (2003), On the generation of secondary microseisms observed in north and central Europe, *J. Geophys. Res*, *108*(B10), 2506, doi:10.1029/2002JB002338.

Friedrich, A., F. Krüger, and K. Klinge (1998), Ocean-generated microseismic noise located with the Gräfenberg array, *J. Seismol.*, *2*, 47–64.

Graham, N. E., and H. F. Diaz (2001), Evidence for intensification of North Pacific winter cyclones since 1948, *Bull. Am. Meteorol. Soc.*, *82*, 1869–1893.

Grevemeyer, I., R. Herber, and H. Essen (2000), Microseismological evidence for a changing wave climate in the northeast Atlantic Ocean, *Nature*, *408*, 349–352.

Harben, P. E., and H. Hjortenberg (1993), Variation in microseism power and direction of approach in northeast Greenland, *Bull. Seismol. Soc. Am.*, *83*, 1939–1958.

Hasselmann, K. (1963), A statistical analysis of the generation of microseisms, *Rev. Geophys.*, *1*, 177–210.

Haubrich, R. A., and K. McCamy (1969), Microseisms: Coastal and pelagic sources, *Rev. Geophys.*, *7*, 539–571.

Junger, S. (1999), *The Perfect Storm*, HarperCollins, New York.

Jurkevics, A. (1988), Polarization analysis of three-component array data, *Bull. Seismol. Soc. Am.*, *78*, 1725–1743.

Kibblewhite, A., and K. Ewans (1985), Wave-wave interactions, microseisms, and infrasonic ambient noise in the ocean, *J. Acoust. Soc. Am.*, *78*, 981–994.

Longuet-Higgins, M. S. (1950), A theory on the origin of microseisms, *Philos. Trans. R. Soc. London*, *243*, 1–35.

McNamara, D. E., and T. J. Owens (1993), Azimuthal shear wave velocity anisotropy in the Basin and Range province using Moho Ps converted phases, *J. Geophys. Res.*, *98*, 12,003–12,017.

Mori, J., H. Kanamori, J. Davis, E. Hauksson, R. Clayton, T. Heaton, L. Jones, and A. Shakal (1998), Major improvements in progress for Southern California earthquake monitoring, *Eos Trans. AGU*, *79*, 217–221.

O'Reilly, W. C., and R. T. Guza (1993), A comparison of two spectral wave models in the Southern California Bight, *Coast. Eng.*, *19*, 263–282.

Tolman, H. L. (1999), User manual and system documentation of WAVEWATCH III, version 1.18, *Tech. Rep. Ocean Modeling Branch Contribution 166*, NOAA/NWS/NCEP.